Comprehensive Performance Evaluation of Sliding-bearing Wind Turbine Gearboxes

Yao Li[1] ✉ – Longsheng Li[1] – Gaoxiang Ni[1] – Xinlong Li[1] ✉ – Jianjun Tan[2] – Kongde He[1]

1 College of Mechanical & Power, China Three Gorges University, China
2 State Key Laboratory of Mechanical Transmission for Advanced Equipment, Chongqing University, China
✉ yao_li_@outlook.com, Xinlongl@163.com

Abstract *Considering the structural characteristics and multi-source excitations of sliding-bearing wind turbine gearboxes, this study constructs a multi-body dynamic model of high-power sliding-bearing wind turbine gearboxes. A comprehensive performance evaluation methodology is proposed, integrating the analytic network process (ANP) with an improved fuzzy comprehensive evaluation (IFCE). A multidimensional comprehensive performance evaluation framework, emphasizing the practicality and cost-effectiveness is developed consisting of target, criterion, and indicator layers. The key evaluation indicators identified within this framework include the main shaft bearing support force, transmission system reliability, load-sharing coefficient, vibration characteristics, and power density. Utilizing ANP and IFCE methodologies the comprehensive performance of two sliding-bearing wind turbine gearboxes is systematically assessed.*

Keywords *sliding-bearing wind turbine gearbox, comprehensive performance evaluation, multidimensional evaluation indicators, analytic network process, fuzzy comprehensive evaluation*

Highlights

- *A rigid-flexible coupling multi-body dynamics model for a high-power sliding-bearing of wind turbine gearboxes (WTGs) is established.*
- *Comprehensive performance evaluation indicators, consisting of 5 primary and 13 secondary indicators, are proposed.*
- *Introduced a comprehensive performance evaluation ANP–IFCE-based method to evaluate WTG performance, focusing on cost and practicality.*

1 INTRODUCTION

Planetary gear trains offer significant advantages, including high-power density, large transmission ratio, and compact structure, making them widely used in wind turbine gearboxes. Traditionally, planetary gear trains often use rolling bearings as supports. However, as wind turbine capacity continues to grow, the gearbox power requirements also increase, exacerbating the challenge of balancing low-cost and high-power-density designs under complex environmental loads. Consequently, wind turbine companies have begun adopting sliding bearings – characterized by their low cost, simplicity and reliability – in wind turbine gearboxes (WTGs). Replacing rolling bearings with sliding bearings significantly reduces the gearbox's size, weight, and cost, while simultaneously enhancing gearbox service life and torque density. Therefore, this study focuses on developing comprehensive performance evaluation methods to validate the actual performance of high-power sliding-bearing WTGs.

In recent years, some scholars have performed performance evaluations of wind turbine gearboxes. Tan et al. [1,2] studied different vibration modes and discussed the impact of internal and external excitations on gearbox dynamic response. Bi et al. [3] proposed a method for identifying fault modes in tooth root cracks using generalized back propagation neural networks. Pan et al. [4] proposed a performance degradation evaluation approach employing complete ensemble empirical mode decomposition with adaptive noise to denoise and fuse vibration signals. Tan et al. [5] analyzed the effects of structural flexibility on the dynamic characteristics of the planetary gear train. Ghane et al. [6] used spectral analysis to obtain characteristic bearing fault signals across six severity levels. Wang [7] proposed a performance analysis method for spiral differential gear trains. Zhao et al. [8] analyzed the influence of tooth flank clearance and eccentricity on the system response. Park et al. [9] built a three-dimensional dynamic model of the wind turbine drivetrain, assessing its dynamic response and tooth contact forces. Shi et al. [10] examined how shaft bending influences rotational and translational motion as well as gear contact forces within transmission systems. Zhao et al. [11] analyzed the dynamic characteristics of a fully flexible wind turbine gearbox, focusing on the component flexibility impact. Wang et al. [12] analyzed the dynamic response of the transmission system of a 10 MW offshore wind turbine transmission system and estimated the 20-year fatigue damage of gears and bearings. Xie et al. [13] studied the effects of time-varying loads, inter-stage gap fluctuations, and crack depth on load-sharing capacity and vibration suppression effectiveness of wind turbines. Xie et al. [14] established a multi-body dynamic model incorporating passive-tuned mass dampers (TMDs) and optimized TMD parameters using genetic algorithms.

Several scholars studied the bearing's performance of WTGs. Koukoura et al. [15] predicted planet bearing failures using vibration data. Fuentes et al. [16] proposed an acoustic-emission method for detecting surface damage in bearings. Keller et al. [17] found that the preloaded tapered roller bearings in WTGs have higher load-sharing capacity than that of cylindrical rolling bearings with bearing clearances, with the expected fatigue life 3.5 times longer. Elasha et al. [18] used a multi-layer neural network model to predict the remaining service life of bearings. Song et al. [19] solved the dynamic load of high-speed shaft bearings using the Newmark integration method and obtained the bearing's fatigue life and dynamic reliability. Mokhtari et al. [20] used vibration and acoustic emission technology to detect radial bearing faults in wind turbine gears and predict the remaining service life of bearings. They built a test bench to conduct experiments. Hagemann et al. [21] found that the bearing design process requires analyzing the distribution of gear meshing loads to determine the critical conditions for bearing operation. At the same time, wear phenomena can improve bearings' circumferential and

axial clearance shapes, significantly reducing localized maximum pressure. König et al. [22] utilized acoustic emission technology to distinguish between critical wear and mixed friction states, applying a data-driven wear monitoring method to predict wear and degradation. Tang et al. [23] coupled a time-varying linear stiffness damping model with an additional eccentricity correction force to establish a planetary gear system dynamic model for WTGs using sliding bearings. Zhao et al. [24] developed a reliability evaluation method for WTG bearings considering the competitive failure between degradation and sudden failure. Dhanola et al. [25] studied the effects of thermal elasticity on the performance parameters of sliding bearings lubricated with degradable nano lubricants. However, most research focuses on WTGs with rolling bearings and needs more quantitative evaluation research on the comprehensive performance of sliding-bearing WTGs. Therefore, conducting comprehensive performance evaluation research on high-power sliding-bearing WTGs is significant.

This contribution establishes a rigid-flexible coupling multi-body dynamics model for a high-power sliding-bearing WTG, considering five primary and thirteen secondary performance indicators. It also proposes a comprehensive performance evaluation method for the sliding-bearing WTGs based on the analytic network process (ANP) and improved fuzzy comprehensive evaluation (IFCE). The remainder of this paper is organized as follows: Section 2 shows the dynamic model of the sliding-bearing WTG. Section 3 gives the performance evaluation of the WTG. Section 4 provides the quantitative analysis of the comprehensive performance of the WTG. Finally, some conclusions are summarised in Section 5.

2 METHODS & MATERIALS

2.1 Structure and Operating Principle of the WTG

The WTG includes a three-stage transmission structure consisting of a low-speed stage, an intermediate stage, and a high-speed stage. The low-speed and intermediate stages are planetary helical gear transmissions, composed of sun gears, planetary gears, planetary carriers, ring gears, and associated components. The high-speed stage utilizes a parallel shaft helical gear transmission, composed of a gear and a pinion. The sliding bearings are applied to support planetary gear shafts. The structural diagram is shown in Fig. 1. The low-speed, high-torque mechanical energy from the main shaft end is first transmitted to the planetary gear system through the low-speed stage planetary carrier. The low-speed stage sun gear meshes with the planet gears transfers motion and force to the intermediate-stage planetary carrier through the low-speed shaft. Similar to the low-speed transmission mode, the intermediate stage planetary gear system transfers motion and force to the high-speed stage gear through its sun gear, which finally drives the pinion and the output shaft. At this point, the low-speed, high-torque input energy has been converted into high-speed, low-torque mechanical energy, which is used to drive the generator for electricity production.

2.2 Sliding Bearing Dynamic Modelling

The planet gear sliding bearings of WTGs often operate under low-speed and heavy-load conditions. During operation, the oil film of the bearings will generate heat due to shear forces and pressure. Consequently, it is necessary to consider the influence of thermal elastic deformation on the bearing behaviour. To this end, the coupled Reynolds equation, temperature control equation, and temperature viscosity equation are applied to calculate the oil film pressure distribution. An iterative calculation method is used to obtain the discrete solutions, from which the oil film thickness, load-bearing capacity, friction power loss, as well as the stiffness and damping of the oil film can be calculated.

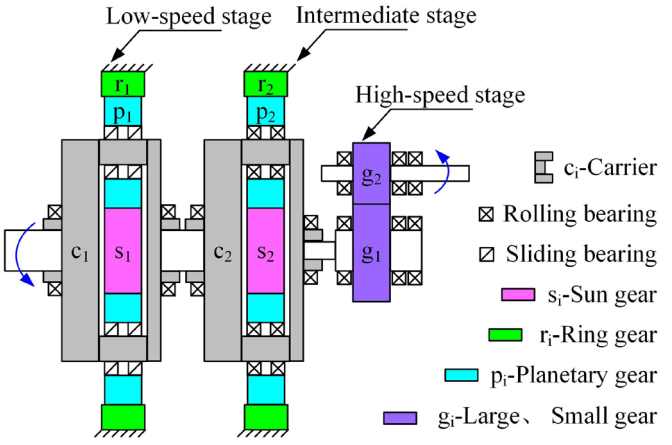

Fig. 1. Structural diagram of sliding-bearing WTGs

The planet gear sliding bearings of WTGs operate in a mixed-friction state under heavy load and low-speed conditions. Considering the influence of surface roughness on the fluid film area, the generalized average Reynolds equation for laminar flow is expanded, and the Reynolds equation is formulated as follows:

$$\frac{\partial}{r_j\partial\phi}\left(\Phi_x^p F_2\frac{\partial p_h}{r_j\partial\phi}\right)+\frac{\partial}{\partial z}\left(\Phi_z^p F_2\frac{\partial p_h}{\partial z}\right)= =U_p\frac{\partial}{r_j\partial\phi}\left(\Theta\left(h-\frac{F_1}{F_0}\right)\right)-\frac{U_p}{2}\frac{\partial\left(\Theta R_q\Phi_x^s\right)}{r_j\partial\phi}, \quad (1)$$

where F_0, F_1, and F_2 represent the lubricant dynamic viscosity coefficient; p_h is the oil film pressure; h is the thickness of oil film at any point; and, Φ_x^p, and Φ_z^p, show the x, z-axis pressure flow factor; Φ_x^s is the shear factor; R_q represents the surface roughness; Θ represents the lubricating oil density, U_p is the planetary shaft speed.

The temperature and viscosity of the lubricating oil are inversely proportional. This relationship can be described using the temperature-viscosity equation, which reflects how the viscosity changes with temperature. The mathematical equation can be expressed as:

$$\eta(T)=\eta_0\left(\frac{T}{T_0}\right)^{-1}, \quad (2)$$

where η and η_0 represent the dynamic viscosity of the lubricating oil when the bearing temperatures are T and To, respectively.

Combining Eqs. (1) and (2), the distribution of oil film pressure can be calculated through the iterative finite difference method. The oil film thickness h can be calculated by:

$$h(\phi,z)=C_R-e\cos(\phi-\gamma) +z\left(-\varphi_x\cos(\phi)+\varphi_y\sin(\phi)\right)+\Delta h(\phi,z), \quad (3)$$

where C_R is the radial clearance; e represents the eccentricity; γ is the attitude angle; ϕ represents the angular coordinate; Δh is the value of the oil film thickness at each point minus the minimum oil film thickness; φ_x and φ_y represent the alignment angles between planet shafts and bearings.

The total load capacity of the bearing can be calculated by Eq. (4).

$$P=\sqrt{P_x^2+P_y^2}, \quad (4)$$

where P_x and P_y are the x- and y-direction components of the radial bearing load capacity.

The dimensionless bearing characteristic C_p usually represents the bearing load capacity, as shown in Eq. (5).

$$C_p = \frac{p_m \psi^2}{\eta \omega}, \tag{5}$$

where ψ is the bearing clearance ratio; ω represents the bearing speed, and p_m is the average pressure of the bearing.

The oil film's stiffness and damping are key components that reflect the bearing's operating state. The oil film stiffness is defined as the derivative of the oil film bearing capacity with respect to the eccentricity, and its mathematical description is given in Eq. (6).

$$\begin{cases} K_{xx} = \dfrac{\partial P_x}{\partial x} = \dfrac{\partial}{\partial x}\displaystyle\int_{-B/2}^{B/2}\int_{\phi_a}^{\phi_b} -p\sin\phi r d\phi dz \\ K_{xy} = \dfrac{\partial P_x}{\partial y} = \dfrac{\partial}{\partial y}\displaystyle\int_{-B/2}^{B/2}\int_{\phi_a}^{\phi_b} -p\sin\phi r d\phi dz \\ K_{yx} = \dfrac{\partial P_y}{\partial x} = \dfrac{\partial}{\partial x}\displaystyle\int_{-B/2}^{B/2}\int_{\phi_a}^{\phi_b} -p\cos\phi r d\phi dz \\ K_{yy} = \dfrac{\partial P_y}{\partial y} = \dfrac{\partial}{\partial y}\displaystyle\int_{-B/2}^{B/2}\int_{\phi_a}^{\phi_b} -p\cos\phi r d\phi dz \end{cases}. \tag{6}$$

Similar to the calculation of the oil film stiffness, the oil film damping is the derivative of bearing capacity with respect to velocity.

Bearings are affected not only by internal excitations, such as thermal elastic deformation and installation errors, but also by external excitations arising from wind speed fluctuation. According to the wind speed statistics from a representative wind farm, a two-parameter Weibull distribution is used to fit the wind speed. The probability density function is given by:

$$f(u) = \frac{k}{c}\left(\frac{u}{c}\right)^{k-1} e^{-\left(\frac{u}{c}\right)^k}, \tag{7}$$

where k = 8.426, c = 1.708. The corresponding cumulative distribution function is:

$$F(u) = 1 - e^{-\left(\frac{u}{c}\right)^k}, \tag{8}$$

where u is the wind speed, k represents the shape parameter, and c is the scale parameter. Considering the wind shear effect, the wind speed at the hub height is calculated by:

$$u_{\text{hub}} = u\left(\frac{z_{\text{hub}}}{z}\right)^{0.2}, \tag{9}$$

where z_{hub} is the hub height, u_{hub} represents the wind speed at the hub, and z is the height at which the wind speed is to be estimated.

The Kaimal model is used to calculate the turbulent wind. The spectral densities of the three spatial components of turbulent wind velocity are given by:

$$S_k(f) = \frac{\dfrac{4\sigma^2 L_k}{u_{\text{hub}}}}{\left(1 + \dfrac{6fL_k}{u_{\text{hub}}}\right)^{\frac{5}{3}}}, \tag{10}$$

where $k = u, v, w$ correspond to the longitudinal, lateral and vertical wind directions; u_{hub} is the average wind speed at the hub height; f is the cyclic frequency; L_k is the integral length scale parameter for each wind component. According to the IEC 61400-1 standard [26], the integral length scales can be expressed as

$$L_k = \begin{cases} 8.10\Lambda_u, & k = u \\ 2.70\Lambda_u, & k = v \\ 0.66\Lambda_u, & k = w \end{cases}, \tag{11}$$

where Λ_u is the turbulence scale coefficient. The correlation model of wind speeds at two points k and h in space is expressed as:

$$S_{k,h}(f) = P_{\text{Coh}}(f)\sqrt{S_{k,k}(f) \cdot S_{h,h}(f)}, \tag{12}$$

where $P_{\text{Coh}}(f)$ is the spatial coherence.

2.3 Dynamic Model of The Sliding-Bearing WTG

Due to the rigid-flexible coupling structure, the sliding-bearing WTG must consider the effects of flexible components on the system's dynamic characteristics. Therefore, the rigid and flexible bodies in the system are modeled according to the ISO 6336 standard [27]. The housing and gears of the gearbox are considered as rigid bodies with six degrees of freedom, while the rolling bearings are represented by equivalent spring-damping model, also with six degrees of freedom to capture coupling effects. In contrast, the carriers and gear shafts are regarded as flexible bodies. The relevant modelling strategies and the degree-of-freedom division of each component are detailed in Table 1.

Table 1. Modeling standards for sliding bearing gearbox

Component	Modeling method	Degrees of freedom
Housing	Flexible body	6 DOF
Planet carrier	Flexible body	6 DOF
Gear shaft	Flexible body	6 DOF
Gear	Rigid body	6 DOF
Generator coupling	Torsional segmented rigid body	Rotational DOF
Generator rotor	Rigid body	6 DOF
Generator stator	Rigid body	6 DOF
Elastic support	Damping nylon element	Translational DOF
Base plate	Rigid body	6 DOF
Bearing	Damping nylon element	Full stiffness matrix

The stiffness is represented by a 6×6 matrix, as shown in Eq. (13). Among them, non-diagonal elements represent the coupling relationship between the stiffnesses.

$$K_{bearing} = \begin{bmatrix} K_x & K_{12} & K_{13} & K_{14} & K_{15} & K_{16} \\ K_{21} & K_y & K_{23} & K_{24} & K_{25} & K_{26} \\ K_{31} & K_{32} & K_z & K_{34} & K_{35} & K_{36} \\ K_{41} & K_{42} & K_{43} & K_\alpha & K_{45} & K_{46} \\ K_{51} & K_{52} & K_{53} & K_{54} & K_\beta & K_{56} \\ K_{61} & K_{62} & K_{63} & K_{64} & K_{65} & K_\gamma \end{bmatrix}, \tag{13}$$

where x, y and z are respectively 3 degrees of translational freedom; α, β, and γ are the rotational degrees of freedom corresponding to the x, y and z directions, respectively.

Gear meshing is one of the primary sources of internal excitation in a gearbox. To model this effect, the slicing method is used to build the gear model, and the finite element method is employed to obtain the meshing stiffness of gear teeth per unit tooth width. Because the number of engaged slices varies during the meshing process, the variation of gear meshing stiffness with the meshing phase can be simulated. Thus, the load distribution along the tooth width direction can be obtained, as shown in Fig. 2.

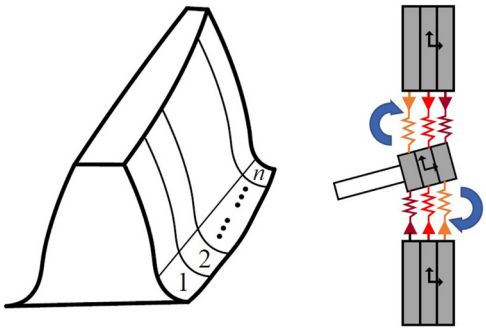

Fig. 2. Schematic of gear slicing

Its meshing stiffness is calculated in accordance with the ISO 6336 standard [27], as follows:

$$c_{\max} = c' C_R, \tag{14}$$

where c' is the meshing stiffness of a single tooth, while C_R is the gear tooth structure coefficient. The calculation formula for the meshing stiffness of a single tooth can be expressed as:

$$c' = c_{\text{th}} C_M C_B \cos\beta, \tag{15}$$

where c_{th} is the theoretical meshing stiffness of a single tooth; C_M is the theoretical correction coefficient; C_B is the basic rack coefficient; β is the helix angle. The theoretical meshing stiffness of a single tooth c_{th} is defined as:

$$c_{\text{th}} = \frac{1}{q}, \tag{16}$$

$$q = 0.04723 + \frac{0.15551}{z_{n1}} + \frac{0.25791}{z_{n2}} - 0.00635x_1 - \frac{0.11654}{z_{n1}} - 0.00193x_2 - \frac{0.24188x_2}{z_{n2}} + 0.00529x_1^2 + 0.00182x_2^2, \tag{17}$$

where z_{n1} and z_{n2} are the equivalent tooth numbers of the driving gear, and the driven gear, respectively; x_1 and x_2 are the modification coefficients of the driving gear, and the driven gear, respectively. The time-varying meshing stiffness function of gears can be expressed as:

$$c(\varphi) = c_{\max}\left[1 - (1 - S_R)\left(\frac{s(\varphi)}{\max(s_{1c}, s_{2c})}\right)^2\right], \tag{18}$$

where $S_R = c_{\min}/c_{\max}$ is the gear stiffness ratio, $s(\varphi) = r_g\varphi$ represents the contact path coordinate, and s_1c and s_2c are the distances from the node along the meshing line to the meshing-in point and meshing-out point, respectively. The calculation formula for transmission error can be expressed as:

$$e_L = \varphi_2 - \left[(\varphi_1 - \varphi_{10})\frac{N_1}{N_2} + \varphi_{20}\right], \tag{19}$$

where φ_{10} and φ_{20} are the initial rotation angles of the driving gear, and the driven gear at the moment of entering meshing, respectively; φ_1 and φ_2 are the rotation displacement angles of the driving gear, and the driven gear, respectively; N_1 and N_2 are the number of teeth of the driving gear, and the driven gear, respectively.

The topological relationship of the sliding-bearing WTG of the floating wind turbine is shown in Fig. 3. It encompasses three key aspects, including: the components, the topological relationships, and the force elements. The components represent the gearbox transmission components, the topological relationships represent the connection relationships and motion constraints among these components, and the force elements represent the interactions between them. Within this system, the components of the sliding-bearing WTG are constrained by both stiffness and damping effects.

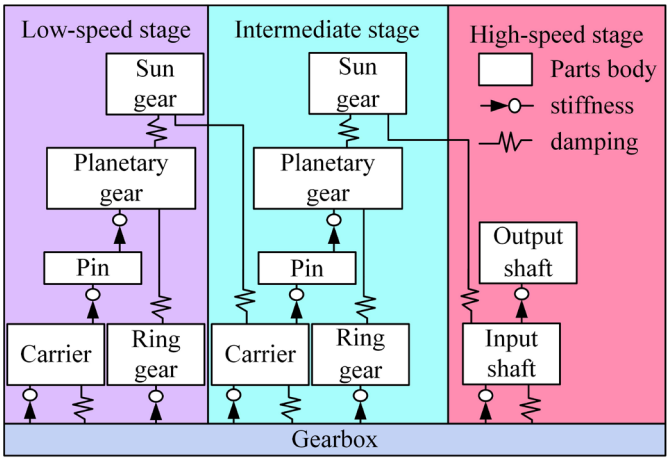

Fig. 3. Topology diagram of sliding-bearing WTGs

According to the connection relationships and topological structure among the transmission components, a multi-body dynamics model of the sliding-bearing WTG is established. Differential equations governing the flexible body motion are established based on the Lagrange multiplier method and modal synthesis method, as shown in Eq. (20). The flexible body modal reduction model is established through the finite element method.

$$\mathbf{M}\ddot{\xi} + \mathbf{M}\dot{\xi} - \frac{1}{2}\left(\frac{\partial M}{\partial \xi}\xi\right)^T\dot{\xi} + \mathbf{K}\xi + f_g + \mathbf{D}\dot{\xi} + \left(\frac{\partial \psi}{\partial \xi}\right)\lambda = \mathbf{Q}, \tag{20}$$

where $\mathbf{M}$ represents the mass matrix, $\mathbf{K}$ is the stiffness matrix, $\mathbf{D}$ represents the modal damping matrix, and f_g represents the generalized gravity.

2.4 Validation of the dynamic model accuracy

To verify the reliability of the multi-body dynamic model, a sliding-bearing wind turbine gearbox case reported in the literature [28], featuring a similar structural configuration and operating conditions, was selected for comparison. Key performance indicators, including the generator rotor speed as well as the vibration acceleration of both the main shaft and the gearbox output shaft, were analysed comparatively.

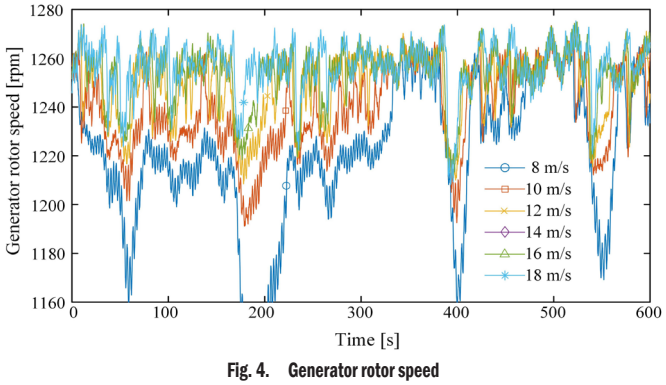

Fig. 4. Generator rotor speed

Figure 4 illustrates the generator speed response of the dynamic model under various wind speeds. The results show that when the average wind speed is 8 m/s, the rotor speed exhibits significant fluctuations, with frequent and noticeable drops. As the wind speed increases, the amplitude of these fluctuations gradually decreases, and the system demonstrates improved operational stability. Once the wind speed reaches 14 m/s or higher, the generator speed stabilizes around 1260 rpm under the influence of pitch control, and the

fluctuations are significantly reduced. This dynamic trend closely aligns with the results reported in literature [28], indicating that the model effectively reflects the system's steady-state behaviour and control response under diverse wind conditions.

Figures 5 and 6 present the main shaft vibration acceleration reported in reference [28] and obtained in the present study, respectively. As observed, both sets of data exhibit a highly consistent trend, showing the amplitude of vibration acceleration progressively increasing with rising wind speed. This trend indicates the significant impact of wind speed on the system's dynamic load and structural response. The developed model accurately captures the dynamic characteristics of the wind turbine gearbox under varying wind speed excitations. These findings verify the validity and reliability of the proposed model in reflecting the actual operational response of sliding-bearing WTGs.

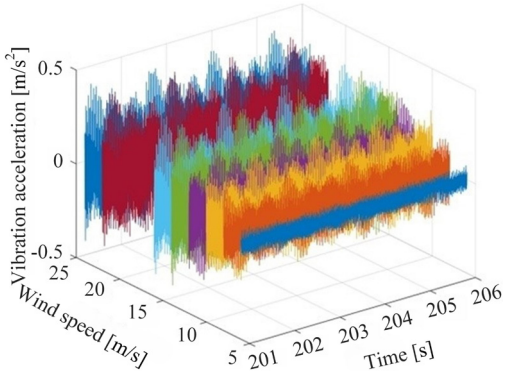

Fig. 5. Main shaft vibration acceleration in reference [28]

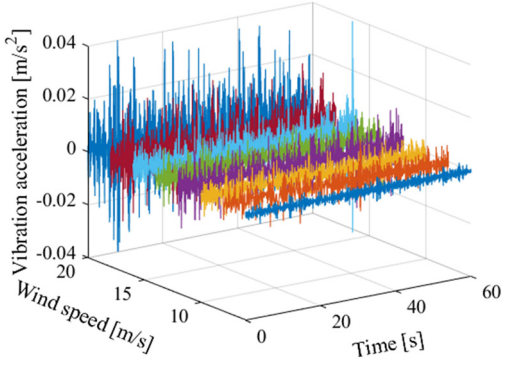

Fig. 6. Main shaft vibration acceleration in the present study

It should be noted that due to differences, the absolute vibration amplitudes arise due to differences in structural dimensions, boundary conditions, and simulation time steps between the model and the literature case. However, the overall trends remain consistent, and the differences are within an acceptable engineering range. The agreement in trend and dynamic behaviour of key indicators further validates the accuracy and reliability of the proposed multibody dynamic model.

3 RESULTS AND DISCUSSION

ANP is suitable for handling complex decision-making problems involving internal dependencies and feedback relationships. It employs a network structure integrating both qualitative and quantitative analysis to accurately describe connections among entities, comprising a control layer as a typical hierarchical structure and a network layer where elements mutually influence and dominate, as illustrated in Fig. 7. Fuzzy comprehensive evaluation (FCE) method uses fuzzy mathematics to comprehensively assess multi-objective problems characterized by uncertainty, establishing corresponding membership functions and conducting quantitative analysis of fuzzy objects through a series of operations and transformations. The ANP-IFCE method combines ANP with the IFCE, classifying various factors of the evaluation object into multiple network levels according to their attributes. Elements within each network level mutually influence and dominate, enabling comprehensive evaluation of each level before proceeding to higher-level synthesis. In the dynamic modelling stage, this method establishes a gear slicing model based on the ISO 6336 standard [27] and calculates local contact stiffness of each tooth segment using the finite element analysis (FEA). By accounting for gear elastic deformation, contact nonlinearity, and local stress concentration, it outperforms traditional empirical formulas, enhancing prediction accuracy for key performance indicators like load distribution and vibration response. In the structural design and comprehensive performance evaluation stages, physical quantities such as contact stress and deformation output by FEA are normalized as inputs to membership functions, reducing subjective scoring interference. Meanwhile, structural coupling relationships revealed by FEA (e.g., meshing errors caused by bearing misalignment) are used to construct the ANP network structure, improving both the logical consistency and causal interpretability of weight allocation.

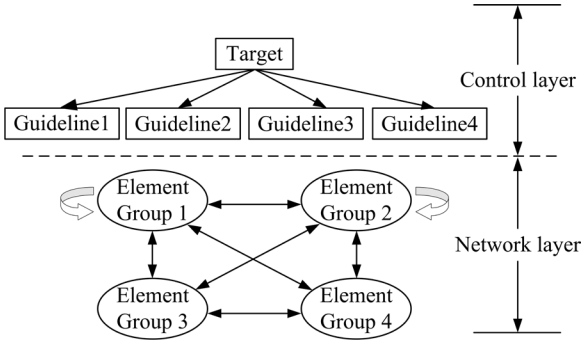

Fig. 7. ANP basic framework

3.1 Performance Evaluation Indexes

Based on the practicality and economy of sliding-bearing WTG, the paper proposes comprehensive performance evaluation indicators, including 5 primary and 13 secondary indicators, as shown in Table 2. U is the comprehensive performance, u_1 is the supporting force of the main shaft bearing, u_2 means the transmission system's reliability, u_3 represents the load-sharing coefficient, u_4 means vibration characteristics, and u_5 is the power density. u_{11}, u_{12} and u_{13} represent the supporting force of the main shaft bearing along the x, y and z-direction, respectively. u_{21} represents the time-varying reliability of bearings, u_{22} and u_{23} are the gear's bending and contact fatigue reliability, respectively. u_{31} and u_{32} are the low-speed and intermediate load-sharing coefficients, respectively. u_{41}, u_{42} and u_{43} represent the vibration acceleration along the x, y and z-direction, respectively. u_{51} is the unit megawatt weight, and u_{52} represents the torque density.

Table 2. Performance evaluation framework for the WTG

Target layer	U				
Criterion layer	u_1	u_2	u_3	u_4	u_5
Indicator layer	u_{11}, u_{12}, u_{13}	u_{21}, u_{22}, u_{23}	u_{31}, u_{32}	u_{41}, u_{42}, u_{43}	u_{51}, u_{52}

3.1.1 Reliability of Gears

Rolling bearings are standardized mechanical components, and their service life generally follows the three-parameter Weibull distribution. Based on the life distribution function, the bearing reliability function can be derived as follows:

$$u_{21}(t)=\exp\left[\left(\frac{t-\gamma}{L_h-\gamma}\right)^{\beta}\cdot\ln 0.9\right], \tag{21}$$

where L_h is the basic rating life, and γ and β represent the position and shape parameters, respectively.

The wear failure is the primary failure mode for sliding bearings. The main factors affecting the performance of sliding bearings are: bearing pressure (p), sliding speed (v), and the value of (pv). The pv value can be calculated as follows:

$$pv=\frac{Fv}{BD}\le[pv], \tag{22}$$

where F is the radial load of sliding bearings, D represents the bearing diameter, B means the effective width of bearings, and $[pv]$ is the allowable value.

According to Archard's wear theory, the wear volume of sliding bearings under normal conditions is linearly proportional to the sliding distance. Therefore, the wear coefficient K is used to estimate the wear volume Δ:

$$\Delta=Kpl=K\frac{F}{DB}l=Kpvt, \tag{23}$$

where K is the wear coefficient.

The actual clearance of the sliding bearing can be determined by the initial bearing clearance (L_0) and the radial wear (Δ), as shown in Eq. (24). Due to factors such as installation error, manufacturing tolerances and varying operating conditions, the allowable clearance of different sliding bearings is random and can be approximated by a normal distribution $L_C \sim N(\mu_{L_C}, \delta_{L_C})$. When the actual clearance L_t exceeds the allowable clearance L_C, the sliding bearing fails due to excessive wear.

$$L_C=L_0+\Delta=L_0+Kpvt, \tag{24}$$

In engineering practice, the allowable clearance, when used as a boundary condition for assessing wear failure, exhibits inherent ambiguity. This ambiguity is most significant near the mean value of the allowable clearance $\overline{L_C}$. Therefore, the descending half-normal distribution function is used to characterize the uncertainty. When the membership degree is 0.5, the mean value of the allowable clearance is taken as the corresponding value, and the membership function can be mathematically described by Eq. (25), as shown in Fig. 8.

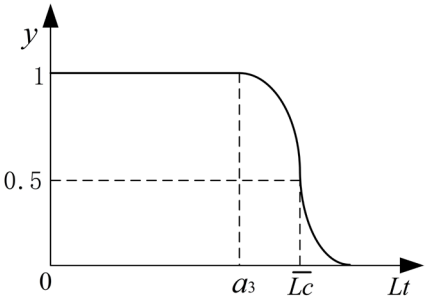

Fig. 8. Schematic diagram of membership function

$$y_i(L_t)=\begin{cases}1 & L_t\le a\\ e^{-\left[\frac{L_t-a}{\delta_{Lc}}\right]} & L_t>a\end{cases}, \tag{25}$$

where L_t is the actual fit clearance, δ_{L_C} represents the allowable clearance variance, $\overline{L_C}$ is the mean allowable gap, a means the fuzzy upper bound, $y(L_C)=0.5$ and $a=\overline{L_C}-\delta_{L_C}/1.2$.

The reliability of the sliding bearing can be calculated by the transcendental function integral formula as shown in Eq. (26).

$$\begin{aligned}u(t)=&\int_{-\infty}^{+\infty}y(Lt)f(Lt)dLt=\Phi\left(\frac{a_3-\overline{Lt}}{\delta Lt}\right)-\Phi\left(\frac{-\overline{Lt}}{\delta Lt}\right)+\\&+\left[1-\Phi\left(\frac{\left(a_3-\overline{Lt}\right)}{\sqrt{2}\delta Lt}\sqrt{\frac{\delta Lc^2}{\delta Lc^2+2\delta Lt^2}}\right)\right]\cdot\\&\cdot\sqrt{\frac{\delta Lc^2}{\delta Lc^2+2\delta Lt^2}}e^{-\left[\frac{\left(a_3-\overline{Lt}\right)^2}{\delta_{Lc}^2+2\delta_{Lt}^2}\right]},\end{aligned} \tag{26}$$

where $f(x)$ is the probability density function, $\Phi(x)$ means the standard normal distribution function, $\overline{L_C}$ represents the mean allowable gap, $\overline{L_t}$ is the actual gap mean, δLC is the allowable gap variance, and δL represents the actual gap variance.

The fuzzy language is used to describe and evaluate gear performance degradation and operation status. Considering the strength degradation, the fuzzy reliability function of gears can be expressed as follows:

$$\begin{aligned}u_{2i}(t)=&\int_{-\infty}^{+\infty}\mu_i\left(\overline{\sigma_i},t\right)g_i(t)d\sigma_i=\\&\frac{1}{0.1r_i(t)}\left[1.1r_i(t)-\overline{\sigma_i}\right]\Phi\left(\frac{1.1r_i(t)-\overline{\sigma_i}}{S_i}\right)-\\&-\frac{1}{0.1r_i(t)}\left[r_i(t)-\overline{\sigma_i}\right]\Phi\left(\frac{r_i(t)-\overline{\sigma_i}}{S_i}\right)+\\&+\frac{S_i}{0.1\sqrt{2\pi}r_i(t)}\cdot\\&\cdot\left[\exp\left(-\frac{(1.1r_i(t)-\overline{\sigma_i})^2}{2S_i^2}\right)-\exp\left(-\frac{(r_i(t)-\overline{\sigma_i})^2}{2S_i^2}\right)\right],\end{aligned} \tag{27}$$

where $\mu_i(.)$ is the membership degree of fuzzy numbers, $g_i(t)$ is the probability distribution function, Si means the standard deviation of allowable stress, $g_i=\overline{\sigma}\ C_i$, $r_i(t)$ is the remaining strength of each gear at time t, $\Phi(.)$ means the standard normal distribution function, and $\overline{\sigma}$ represents the mean stress.

3.1.2 Load-sharing Characteristics

Due to uneven load distributions, the planetary gear train often cannot fully demonstrate its advantages, which seriously affects its working performance and service reliability. A load-sharing coefficient closer to 1 indicates a more uniform load distribution among the planetary gears and thus a higher system load capacity. The closer the load-sharing coefficient is to 1, indicates a more uniform load distribution among the planetary gears and thus a stronger system load capacity. In order to quantitatively evaluate the load-sharing characteristics of the planetary gear train of the WTG, the load-sharing coefficient can be defined as:

$$u_{3i}=\frac{1}{2}\left(\frac{N\times F_{RP_{\max}}}{\sum_i^n F_{RPi_{\max}}}+\frac{N\times F_{SP_{\max}}}{\sum_i^n F_{SPi_{\max}}}\right), \tag{28}$$

where u_{31} and u_{32} represent the load-sharing coefficients for the first and second planetary gear transmissions, $F_{RPi_{\max}}$ and $F_{SPi_{\max}}$ are the maximum dynamic meshing forces of the i^{th} planet gear of the

planetary gear train (i = 1,2, …, N), $F_{RP_{max}}$ and $F_{SP_{max}}$ represent the maximum dynamic meshing forces for the ring-planet gear pair and sun-planet gear pair.

3.1.3 Power Density

Torque density is often used to measure the transmission capacity of a gearbox. A higher torque density means that the gearbox can withstand greater torque load relative to its size. Defined as the torque per unit volume, torque density is typically used to evaluate the performance and efficiency of a transmission system. The torque density u_{51} can be expressed as:

$$u_{51} = \frac{T}{V}, \tag{29}$$

where T is the gearbox torque, and V represents the gearbox volume. The unit megawatt weight is an important indicator used to measure the power generation capacity of wind turbines. A higher value indicates a stronger power output capability relative to the turbine's weight. This characteristic is commonly defined as the power-to-weight ratio (PWR). Therefore, the specific calculation formula of the PWR (R_{52}) can be expressed as:

$$u_{52} = \frac{P}{M}, \tag{30}$$

where P is the generator power, and M represents the gearbox density.

3.2 Construction of the ANP Supermatrix

ANP consists of the control layer and the network layer, where the control layer follows an atypical hierarchical structure, while the elements in the network layer influence each other. ANP is mainly divided into problem description and analysis, construction of ANP hierarchical structure, construction of judgment matrix, consistency test of judgment matrix, and determination of the weight of the basic elements within the supermatrix and weighted supermatrix to the overall goal.

Table 3. Judgment scale of the index importance

Scale value	Description
1	The element i is equally essential as the element j
3	The element i is slightly more essential than the element j
5	The element i is more essential than the element j
7	The element i is much more essential than the element j
9	The element i is the most essential than the element j
2, 4, 6, 8	The median of the two adjacent judgments mentioned above

The ANP evaluation indicator network model is built with the target layer serving as the control layer, while the criterion layer and indicator layer are the network layer, as shown in Table 3. Assume that the control layer elements of ANP are represented as: P_1, P_2, …, P_m, and the first-level indicators of the network layer are denoted as: R_1, R_2, …, R_5, where R_i contains the second-level indicators R_{i1}, R_{i2}, …, R_{in}.

Table 4. Average random consistency indicator

n	1	2	3	4	5	6	7	8	9	10
RI	0	0	0.58	0.90	1.12	1.24	1.32	1.41	1.45	1.49

Taking the control layer element P_S (S = 1, 2, …, m) as the criterion, and the element R_{jk} (k = 1, 2, …, n_j) within R_j (j = 1, 2, …, 4) as the secondary criterion, the elements in R_i are compared according to their influence on R_{jk}. Based on these comparisons, the nine-level scaling method is used to construct the corresponding judgment matrix $\mathbf{L}$, where the scoring scale of the nine-level scaling method is shown in Table 4.

$$\mathbf{L} = \begin{bmatrix} l_{11} & l_{12} & \cdots & l_{1n_i} \\ l_{21} & l_{22} & \cdots & l_{2n_i} \\ \vdots & \vdots & \ddots & \vdots \\ l_{n_i1} & l_{n_i2} & \cdots & l_{n_in_i} \end{bmatrix}. \tag{31}$$

Since the construction of the judgment matrix involves subjective assessments, it is necessary to test its consistency to ensure the evaluation results' accuracy. To this end, the consistency ratio (CR) of the judgment matrix calculated as follows:

$$CI = \frac{\lambda_{\max} - n}{n-1}, \tag{32}$$

$$CR = \frac{\lambda_{\max} - n}{RI(n-1)}, \tag{33}$$

where CI is the consistency indicator, RI is a random consistency index (with values shown in Table 3), n represents the order of the judgment matrix, and $\lambda_{\max}$ is the maximum eigenvalue of the judgment matrix. When n = 0, 1, and CI = 0, the judgment matrix has complete consistency; when $n \geq 2$, and $CR < 0.1$, the judgment matrix can be considered to have satisfactory consistency; otherwise, adjustments are required.

Based on the survey results, a judgment matrix is formed. After passing the consistency test, the judgment matrix can be identified as an unweighted supermatrix $\mathbf{W}_{ij}$, as follows:

$$\mathbf{W}_{ij} = \begin{bmatrix} w_{i1}^{j1} & w_{i1}^{j2} & \cdots & w_{i1}^{jn_j} \\ w_{i2}^{j1} & w_{i2}^{j2} & \cdots & w_{i2}^{jn_j} \\ \vdots & \vdots & \ddots & \vdots \\ w_{in_j}^{j1} & w_{in_j}^{j2} & \cdots & w_{in_j}^{jn_j} \end{bmatrix}, \tag{34}$$

where the column vector of $\mathbf{W}_{ij}$ represents the ranking vector of the influencing factors R_{i1}, R_{i1}, …, R_{ini}. Within the factor layer of the evaluation index, this vector reflects the degree of influence of the factors R_{j1}, R_{j2}, …, R_{jnj} in R_j.

By comparing the importance of the criterion layer indicators R_i with R_j (i, j = 1, 2, …, 5) in the evaluation indicators, a weighted matrix $\mathbf{A}$ of the criterion-layer indicators can be obtained by pairwise comparison, which is expressed as follows:

$$\mathbf{A} = \begin{bmatrix} a_{11} & a_{12} & \cdots & a_{1n} \\ a_{21} & a_{22} & \cdots & a_{2n} \\ \vdots & \vdots & \ddots & \vdots \\ a_{n1} & a_{n2} & \cdots & a_{nn} \end{bmatrix}. \tag{35}$$

By applying the weighted matrix $\mathbf{A}$ to weight the unweighted supermatrix $\mathbf{W}_{ij}$, the weighted supermatrix $\bar{\mathbf{W}}_{ij}$ is obtained, which can be expressed as follows:

$$\bar{\mathbf{W}}_{ij} = \begin{bmatrix} a_{11}w_{11} & a_{12}w_{12} & \cdots & a_{1n}w_{1n} \\ a_{21}w_{21} & a_{12}w_{22} & \cdots & a_{2n}w_{2n} \\ \vdots & \vdots & \ddots & \vdots \\ a_{n1}w_{n1} & a_{n2}w_{n2} & \cdots & a_{nn}w_{nn} \end{bmatrix}, \tag{36}$$

where $\bar{\mathbf{W}}_{ij} = a_{ij}w_{ij}$, I =1, 2, …, n, j = 1, 2, …, n ($n \geq 6$).

The normalized form of the weighted supermatrix yields the limit supermatrix $\mathbf{W}_{\infty}$, whose column vector represents the weight vector R_{inj} of the comprehensive performance evaluation factor index $\mathbf{W}'$ for the sliding-bearing wind turbine gearbox, which is expressed as follows:

$$\mathbf{W}' = (W_{11}, W_{12}, \cdots, W_{ini}, \cdots, W_{NnN})^{\mathrm{T}}. \tag{37}$$

The normalized weight vector of each index R_{ij} within its corresponding criterion layer index R_i is denoted as $\mathbf{W}'_i$, which is expressed as follows:

$$\mathbf{W}_i^{'} = (W_{i1}^{'}, W_{i2}^{'}, \cdots, W_{ini}^{'})^{\mathrm{T}}. \tag{38}$$

3.3 Improved Performance Evaluation Method for the WTG

The evaluation factors represent the properties and performance of the evaluation target, while the evaluation level indicates the degree to which these factors influence the target. According to the complexity of the target, the factor set $U = (u_1, u_2, \ldots, u_m)$, and the evaluation set $V = (v_1, v_2, \ldots, v_n)$ are determined. Membership functions reflect the relationship between evaluation factors and evaluation levels. Correctly selecting the membership function is critical to ensuring the accuracy of fuzzy comprehensive evaluation. Thus, this study uses the compound membership function to improve the credibility of each indicator's membership function.

The corresponding membership function is selected according to the characteristics of the evaluation index. The single-factor judgment is then performed on the factor set u_i ($i = 1, 2, \ldots, m$) to obtain the membership rij of ui with respect to the evaluation level v_j ($j = 1, 2, \ldots, n$). Following this, the ui judgment set is expressed as $r_i = (r_{i1}, r_{i2}, \ldots, r_{ini})$. By repeating this process for all factors, the whole evaluation matrix **R** can be constructed.

$$R = \begin{bmatrix} r_{11} & r_{12} & \cdots & r_{1n} \\ r_{21} & r_{22} & \cdots & r_{2n} \\ \vdots & \vdots & \ddots & \vdots \\ r_{m1} & r_{m2} & \cdots & r_{mn} \end{bmatrix}. \tag{39}$$

Assume that the membership values of an indicator in n membership functions are $r_1, r_2, \ldots, r_n$, and the variances of the errors relative to $\bar{r}$ are $\sigma_{11}, \sigma_{12}, \ldots, \sigma_{nn}$. The errors among the membership degrees corresponding to the membership functions are unrelated. Given the condition $\Sigma\omega_i = 1$, the Lagrange multiplier is employed to minimize $Var(e^c)$. The weights of various membership functions are obtained as follows:

$$\omega_i = \frac{1}{\sigma_{ii}\left(\frac{1}{\sigma_{11}} + \frac{1}{\sigma_{22}} + \cdots + \frac{1}{\sigma_{nn}}\right)}. \tag{40}$$

From Eq. (40), it can be observed that the closer the membership value is to the average value, the larger its corresponding weight becomes. Therefore, the compound membership function can be calculated by:

$$r_c = \omega_1 r_1 + \omega_2 r_2 + \cdots + \omega_n r_n. \tag{41}$$

3.4 Comprehensive Performance Evaluation of Sliding-Bearing WTGs

According to the evaluation system built in Section 3, the first-level indicators are considered independently and only affected by their second-level indicators. The second-level indicators have either unidirectional or bidirectional influence on each other. By taking the target layer as the control layer in ANP, and the criterion layer and the indicator layer as the network layer (as listed in Table 5), an ANP evaluation indicator network model is constructed, as shown in Fig. 9.

Based on the ANP model for the comprehensive performance evaluation of sliding-bearing WTGs, the expert scoring method is adopted to determine the corresponding weights of indicators at each level. The first-level indicators are regarded as independent of one another and are scored according to the nine-level scaling method. This scoring yields the judgment matrix of the first-level indicators in the control layer, as shown in Table 5.

From Eqs. (32) and (33), the following results are obtained: $\lambda_{max} = 5.24$, $CI = 0.059$, $RI = 1.12$, $CR = 0.053 < 0.1$. Thus, the judgement matrix passed the consistency requirement. The indicator weights of the network layer are then determined based on the importance of the first-level indicators. At this stage, the mutual influences among the elements of the network layer under each first-level indicator need to be considered. The judgment matrix for the second-level indicators of the network layer is constructed through the same method applied for the first-level indicator weights of the control layer, followed by a consistency test. As an example, the reliability indicator is shown in Table 6.

Table 5. Judgment matrix and weight vectors of the first-level indicators in control layer

	R_1	R_2	R_3	R_4	R_5	W
R_1	1	1/3	1	1	1/4	0.096
R_2	3	1	5	3	1/2	0.312
R_3	1	1/5	1	2	1/2	0.128
R_4	1	1/3	1/2	1	1/4	0.086
R_5	4	2	5	4	1	0.378

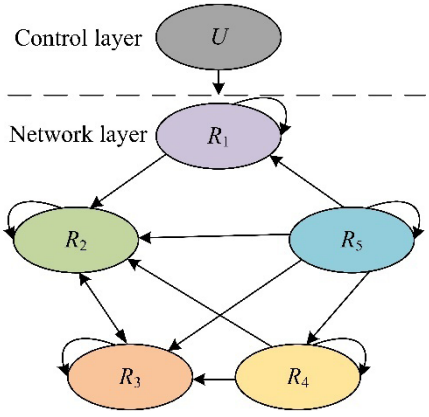

Fig. 9. ANP model for the comprehensive performance of sliding-bearing WTGs

Table 6. Judgment matrix and weight vector of the system reliability

	R_{21}	R_{22}	R_{23}	W
R_{21}	1	2	1	0.411
R_{22}	1/2	1	1	0.261
R_{23}	1	1	1	0.328

Table 7. Weights for comprehensive performance evaluation of sliding-bearing WTGs

First-level indicators	Indicator weight	Second-level indicators	Local weight
R_1	0.096	R_{11}	0.224
		R_{12}	0.369
		R_{13}	0.406
R_2	0.312	R_{21}	0.411
		R_{22}	0.261
		R_{23}	0.328
R_3	0.128	R_{31}	0.500
		R_{32}	0.500
R_4	0.086	R_{41}	0.249
		R_{42}	0.326
		R_{43}	0.426
R_5	0.378	R_{51}	0.500
		R_{52}	0.500

From Eqs. (32) and (33), the following results are obtained: $\lambda_{max} = 3.05$, $CI = 0.046$, $RI = 0.58$, $CR = 0.046 < 0.1$. Thus, the judgement matrix passed the consistency requirements. The remaining secondary indicators of the network layer are then calculated sequentially, and the weighted supermatrix and the limit supermatrix are calculated to obtain the relative weights of the secondary indicators as well as the comprehensive performance evaluation weights of the WTGs, as shown in Table 7. The evaluation criteria are determined according to the performance levels, and a comment set is established, as shown in Table 8.

Table 8. Evaluate the level of membership

Performance level	Inferior V_1	General V_2	Good V_3	Excellent V_4
Evaluation criterion	0 to 25	25 to 50	50 to 75	75 to 100

Then, the membership degree matrix is constructed according to Subsection 3.3. The matrix elements represent the membership degree of each risk factor with respect to each level in the evaluation set. Let the membership vector of risk factor U_i to the judgment set be defined as $V_i = \{V_{i1}, V_{i2}, V_{i3}, V_{i4}\}$. Based on this, the membership degree values of the comprehensive performance indicators for the 6.2 MW sliding-bearing WTG are obtained under three functions, as shown in Table 9.

Table 9. Membership degree of performance indicators for the 6.2 MW sliding-bearing WTG

Indicator factors	Membership function 1/2/3			
	Inferior	General	Good	Excellent
R_{11}	0.00/0.00/0.00	0.00/0.00/0.00	0.67/0.45/0.30	0.33/0.55/0.70
R_{12}	0.00/0.00/0.00	0.00/0.00/0.10	0.50/0.70/0.75	0.50/0.30/0.15
R_{13}	0.00/0.00/0.00	0.10/0.05/0.25	0.90/0.80/0.75	0.00/0.15/0.00
R_{21}	0.00/0.00/0.00	0.00/0.20/0.50	0.70/0.60/0.50	0.30/0.20/0.00
R_{22}	0.00/0.00/0.00	0.00/0.00/0.10	0.15/0.40/0.50	0.85/0.60/0.40
R_{23}	0.00/0.10/0.40	0.50/0.60/0.50	0.50/0.30/0.10	0.00/0.00/0.00
R_{31}	0.00/0.00/0.00	0.00/0.00/0.00	0.10/0.25/0.50	0.90/0.75/0.50
R_{32}	0.00/0.00/0.00	0.00/0.00/0.20	0.30/0.60/0.60	0.70/0.40/0.20
R_{41}	0.00/0.00/0.00	0.00/0.00/0.00	0.10/0.33/0.20	0.90/0.67/0.80
R_{42}	0.00/0.00/0.00	0.00/0.00/0.00	0.33/0.20/0.50	0.67/0.80/0.50
R_{43}	0.00/0.00/0.00	0.00/0.20/0.00	0.50/0.60/0.95	0.50/0.20/0.05
R_{51}	0.00/0.00/0.00	0.10/0.20/0.20	0.40/0.50/0.70	0.50/0.30/0.10
R_{52}	0.00/0.00/0.00	0.10/0.20/0.20	0.40/0.50/0.70	0.50/0.30/0.10

Following this, the variance-covariance method was applied to obtain the combined membership degree values of the comprehensive performance indicators of the 6.2 MW sliding-bearing WTG. Similarly, the combined membership degree values for the 10 MW sliding-bearing WTG were also obtained, as shown in Table 10. and illustrated in Fig. 10.

Table 10. Membership degree of comprehensive performance indicators for sliding-bearing wind turbine gearboxes

Indicator factors	6.2/10 MW sliding-bearing WTGs			
	Inferior	General	Good	Excellent
R_{11}	0.00/0.00	0.00/0.00	0.46/0.17	0.54/0.83
R_{12}	0.00/0.00	0.01/0.01	0.68/0.36	0.31/0.63
R_{13}	0.00/0.00	0.08/0.02	0.81/0.45	0.11/0.53
R_{21}	0.00/0.00	0.21/0.28	0.60/0.43	0.19/0.29
R_{22}	0.00/0.00	0.01/0.00	0.39/0.49	0.61/0.51
R_{23}	0.13/0.31	0.57/0.48	0.30/0.21	0.00/0.00
R_{31}	0.00/0.00	0.00/0.00	0.26/0.41	0.74/0.59
R_{32}	0.00/0.00	0.03/0.03	0.56/0.82	0.42/0.15
R_{41}	0.00/0.00	0.00/0.00	0.28/0.34	0.72/0.66
R_{42}	0.00/0.00	0.00/0.00	0.26/0.52	0.74/0.48
R_{43}	0.00/0.00	0.15/0.39	0.63/0.50	0.22/0.11
R_{51}	0.00/0.00	0.19/0.40	0.51/0.48	0.30/0.12
R_{52}	0.00/0.00	0.19/0.40	0.51/0.48	0.30/0.12

Matrix multiplication is used to perform fuzzy transformation and calculate the fuzzy comprehensive evaluation vector **B**.

$$\mathbf{B} = WR_2 = \begin{bmatrix} 0.00 & 0.04 & 0.68 & 0.28 \\ 0.04 & 0.28 & 0.45 & 0.24 \\ 0.00 & 0.01 & 0.41 & 0.58 \\ 0.00 & 0.06 & 0.42 & 0.52 \\ 0.00 & 0.19 & 0.51 & 0.30 \end{bmatrix}.$$

Afterwards, the secondary comprehensive evaluation is performed to obtain the final fuzzy comprehensive evaluation vector $\mathbf{B}_p$.

$$\mathbf{B}_p = \mathbf{BW} = [0.01 \quad 0.17 \quad 0.49 \quad 0.33].$$

Lastly, the comprehensive performance evaluation value P_1 for the 6.2 MW sliding-bearing WTG is calculated using the formula below.

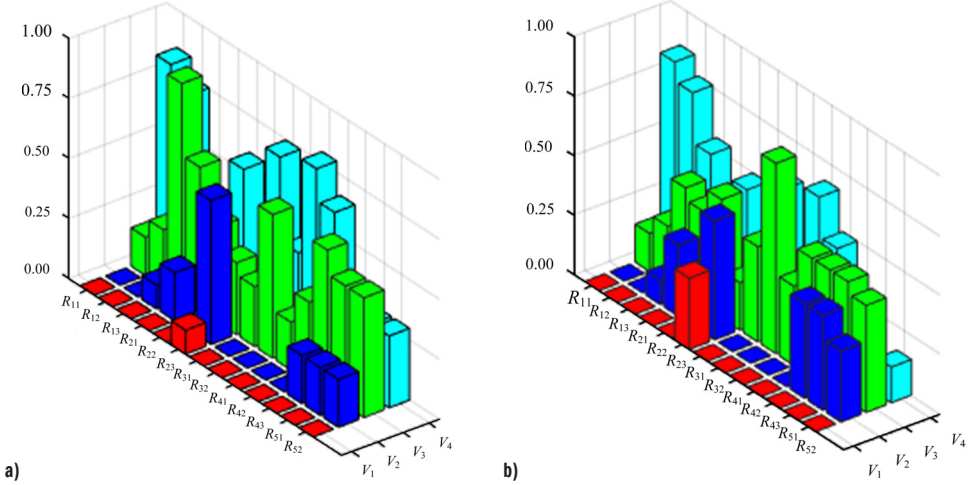

Fig. 10. Membership degree of sliding-bearing WTGs: a) 6.2 MW sliding-bearing WTG, and b) 10 MW sliding-bearing WTG

$$P_1 = [25 \quad 50 \quad 75 \quad 100] \cdot \begin{bmatrix} 0.01 \\ 0.17 \\ 0.49 \\ 0.33 \end{bmatrix} = 78.35.$$

According to the membership degree of performance indicators shown in Table 9, the 6.2 MW sliding-bearing WTG is evaluated as having "excellent" performance. In the same way, the comprehensive performance evaluation value P2 of the 10 MW sliding-bearing WTG is obtained. Thus, the performance of this 10 MW sliding-bearing WTG is evaluated as having "good" performance based on the membership degree of performance indicators, shown in Table 9.

$$P_2 = [25 \quad 50 \quad 75 \quad 100] \cdot \begin{bmatrix} 0.03 \\ 0.25 \\ 0.45 \\ 0.26 \end{bmatrix} = 73.40$$

To verify the reliability of the evaluation method, a sensitivity analysis was carried out on the weights of key indicators in the ANP-IFCE-based evaluation framework. Referencing the requirements of ISO 12100 [29] for parameter perturbation verification of complex systems, a hybrid sensitivity analysis method combining single-factor weight fluctuation testing with multi-factor superposition perturbation was adopted to investigate the response of comprehensive performance evaluation results to index weight perturbations. The first-level index R_5 with the highest weight (power density, weight 0.378) and the second-highest R_2 (reliability, weight 0.312) are selected to apply ±20 % weight perturbation, respectively. The weights of the remaining indicators are proportionally normalized to keep the total weight sum remained equal to 1. Keeping the membership matrix **B** unchanged, the fuzzy comprehensive evaluation result vector $\mathbf{B}'_P$ and the comprehensive performance evaluation value P' of the sliding bearing wind turbine gearbox were calculated after adjusting the weights. The summary results are shown in Table 11.

Table 11. Comparison of fluctuations in comprehensive evaluation value P of 6.2 MW and 10 MW sliding bearing WTGs under ANP index weight adjustment

Adjustment method	6.2 MW		10 MW	
	P'	Variation range [%]	P'	Variation range [%]
Original value	78.35	–	73.40	–
R_5 +20 %	79.25	+1.15	75.50	+2.86
R_2 –20 %	78.25	–0.13	75.00	+2.18
R_5 +20 %, R_2 –20 %	79.75	+1.79	75.75	+3.20

Within the ±20 % weight disturbance range, the comprehensive evaluation value P of the 6.2 MW sliding-bearing wind turbine gearbox fluctuates by no more than +1.79 %, while that of the 10 MW model fluctuates no more than +3.20 %. According to the standard verification procedure of multi-criteria evaluation models, the fluctuation verification of the comprehensive evaluation value P for both 6.2 MW and 10 MW sliding-bearing wind turbine gearboxes shows that all P value fluctuations remain within ±5 %, demonstrating the reliability of the ANP-IFCE model.

4 CONCLUSIONS

To address the lack of systematic performance evaluation indicators and methods for high-power sliding-bearing wind turbine gearboxes, this paper proposes a comprehensive performance evaluation method that integrates ANP and improved FCE. By combining a multi-layer network structure with fuzzy logic, the framework enables coupling modelling and weight quantification among multiple indicators, thereby overcoming the limitations of traditional AHP and single FCE in dealing with inter-indicator correlations and subjective bias. A unified quantitative scoring mechanism is established to support horizontal comparison among different gearbox models as well as customized selection, facilitating structural optimization and multi-working condition adaptive design. Furthermore, dynamic indicators such as load-sharing performance, bearing force, and vibration characteristics are introduced to effectively identify structural risks, evaluate design rationality, and improve the prediction ability at the design stage and thereby improving operational reliability. The main conclusions are obtained as follows:

1. The importance of the first-level indicators for comprehensive performance evaluation of sliding-bearing WTGs is ranked in descending order as follows: power density, reliability, load-sharing performance, support force of main shaft bearings, and vibration characteristics. Among these, both weights of power density and reliability exceeding 30 %, indicating that improvements in these two factors are the most critical for enhancing the overall performance of WTGs.
2. By applying the ANP-IFCE method, which comprehensively considers the mutual influences between various indicators, several secondary factors are identified as key to performance improvement. These include the bearing support force along the z-direction, dynamic reliability of bearings, load-sharing coefficient of the low-speed stage, load-sharing coefficient of the intermediate stage, vibration acceleration along the y-direction, weight per megawatt and torque density. Strengthening these factors is particularly effective in enhancing the comprehensive performance of sliding-bearing WTGs.
3. The comparative evaluation between the 6.2 MW WTG and 10 MW WTG reveals that the 6.2 MW model performs better in terms of reliability, load-sharing performance, vibration characteristics, and power density, but is slightly weaker in the support forces of the main shaft bearing. On balance, the overall comprehensive performance of the 6.2 MW WTG is superior to that of the 10 MW WTG model, confirming its advantages in structural design and operational efficiency.

References

[1] Tan, J., Zhu, C., Song, C., Xu, X. Study on the dynamic modeling and natural characteristics of wind turbine drivetrain considering electromagnetic stiffness. *Mech Mach Theory* 134 541-561 (2019) **DOI:10.1016/j.mechmachtheory.2019.01.015**.

[2] Tan, J., Zhu, C., Song, C., Han, H., Li, Y. Effects of flexibility and suspension configuration of main shaft on dynamic characteristics of wind turbine drivetrain. *Chin J Mech Eng* 32 36 (2019) **DOI:10.1186/s10033-019-0348-4**.

[3] Bi, Y., Zhu, C., Tan, J., Song, H., Du, X. Influence of tooth root crack on dynamic characteristics of wind turbine gearbox high-speed stage and failure mode identification. *Acta Energ Solar Sin* 43 284-292 (2022) **DOI:10.19912/j.0254-0096.tynxb.2020-1251**.

[4] Pan, Y., Hong, R., Chen, J., Singh, J., Jia, X. Performance degradation assessment of a wind turbine gearbox based on multi-sensor data fusion. *Mech Mach Theory*, 137 509-526 (2019) **DOI:10.1016/j.mechmachtheory.2019.03.036**.

[5] Tan, J., Li, H., Zhu, C., Song, C. Study on dynamics characteristics of planetary gear train in wind turbine gearboxes considering flexible structures. *J Vibr Eng*, 36 1191-1203 (2023) **DOI:10.16385/j.cnki.issn.1004-4523.2023.05.002**.

[6] Ghane, M., Nejad, A.R., Blanke, M., Gao, Z., Moan, T. Diagnostic monitoring of drivetrain in a 5 MW spar-type floating wind turbine using Hilbert spectral analysis. *Energ Proced* 137 204-213 (2017) **DOI:10.1016/j.egypro.2017.10.374**.

[7] Wang, C. Study on dynamic performance and optimal design for differential gear train in wind turbine gearbox. *Renew Energy* 221 119776 (2024) **DOI:10.1016/j.renene.2023.119776**.

[8] Zhao, X., Chen, C.Z., Liu, J. Gu, Q. Nonlinear dynamic response analysis of high-level wind turbine gearbox transmission system considering eccentricity. *J Solar Energ* 41 98-108 (2020) **DOI:10.19912/j.0254-0096.2020.03.014**.

[9] Park, Y., Park, H., Ma, Z., You, J., Shi, W. Multibody dynamic analysis of a wind turbine drivetrain in consideration of the shaft bending effect and a variable gear mesh including eccentricity and nacelle movement. *Front Energy Res* 8 604414 (2021) **DOI:10.3389/fenrg.2020.604414**.

[10] Shi, W., Park, Y., Park, H., Ning, D. Dynamic analysis of the wind turbine drivetrain considering shaft bending effect. *J Mech Sci Technol* 32 3065-3072 (2018) **DOI:10.1007/s12206-018-0609-7**.

[11] Zhao, Y., Wei, J., Zhang, S., Xu, Z., Guo, J., Ji, K. Study of effect of structural flexibility on dynamic characteristics of large-scale wind turbine gear transmission system. *Acta Energ Solar Sin* 42 174-182 (2021) **DOI:10.19912/j.0254-0096.tynxb.2019-1433**.

[12] Wang, S., Nejad, A.R., Moan, T. On design, modelling, and analysis of a 10-MW medium-speed drivetrain for offshore wind turbines. *Wind Energy*, 23 1099-1117 (2020) **DOI:10.1002/we.2593**.

[13] Xie, F., Sun, Y., Wu, S., Zhang, Q., Li, X. Research on load sharing performance of wind turbine gearbox involving multiple-errors and tooth crack. *J Mech Sci Technol* 36 4395-4408 (2022) **DOI:10.1007/s12206-022-0804-4**.

[14] Xie, S., Jin, X., He, J. Structural vibration control for offshore floating wind turbine including drivetrain dynamics analysis. *J Renew Sustain Ener* 11 023304 (2019) **DOI:10.1063/1.5079427**.

[15] Koukoura, S., Carroll, J., McDonald, A., Weiss, S. Wind turbine gearbox planet bearing failure prediction using vibration data. *J Physics Conf Ser* 1104 012016 (2018) **DOI:10.1088/1742-6596/1104/1/012016**.

[16] Fuentes, R., Dwyer-Joyce, R., Marshall, M., Wheals, J., Cross, E. Detection of sub-surface damage in wind turbine bearings using acoustic emissions and probabilistic modelling. *Renew Energ* 147 776-797 (2020) **DOI:10.1016/j.renene.2019.08.019**.

[17] Keller, J., Guo, Y., Zhang, Z., Lucas, D. Comparison of planetary bearing load-sharing characteristics in wind turbine gearboxes. *Wind Energ Sci* 3 947-960 (2018) **DOI:10.5194/wes-3-947-2018**.

[18] Elasha, F., Shanbr, S., Li.X., Mba, D. Prognosis of a wind turbine gearbox bearing using supervised machine learning. *Sensors* 19 3092 (2019) **DOI:10.3390/s19143092**.

[19] Song, L., Cui, Q., Jin, P., Zhou, J. High speed bearing fatigue life and reliability analysis of wind turbine gearbox under random load. *Acta Energ Solar Sin* 44 437-444 (2023) **DOI:10.19912/j.0254-0096.tynxb.2022-0562**.

[20] Mokhtari, N., Grzeszkowski, M., Guhmann, C. Vibration signal analysis for the lifetime-prediction and failure detection of future turbofan components. *Tech Mech E J Eng Mech* 37 422-431 (2017) **DOI:10.24352/UB.OVGU-2017-118**.

[21] Hagemann, T., Ding, H., Radtke, E., Schwarze, H. Operating behavior of sliding planet gear bearings for wind turbine gearbox applications part II: impact of structure deformation. *Lubricants* 9 98 (2021) **DOI:10.3390/lubricants9100098**.

[22] Konig, F., Marheineke, J., Jacobs, G., Sous, C., Zuo, M.J., Tian, Z. Data-driven wear monitoring for sliding bearings using acoustic emission signals and long short-term memory neural networks. *Wear* 476 203616 (2021) **DOI:10.1016/j.wear.2021.203616**.

[23] Tang, H., Tan, J., Li, H., Zhu, C., Ye, W., Sun, Z. Research on dynamic modeling and decoupling methods of planetary gear trains in wind turbine gearboxes with journal bearings. *Chin Mech Eng* 35 591 (2024) **DOI:10.3969/j.issn.1004-132X.2024.04.003**.

[24] Zhao, Q. Yuan, Y., Sun, Wang, W., Fan, P., Zhao, J. Remaining useful life analysis of gearbox bearing of wind turbines based on competition failure. *Acta Energ Solar Sin* 42 438-444 (2021) **DOI:10.19912/j.0254-0096.tynxb.2018-1356**.

[25] Dhanola, A., Garg, H.C. Thermo-elasto-hydrodynamic (TEHD) study of journal bearing lubricated with biodegradable nanolubricant. *J Braz Soc Mech Sci*, 43 69 (2021) **DOI:10.1007/S40430-021-02801-3**.

[26] IEC 61400-1:2019. *Wind Energy Generation Systems - Part 1: Design Requirements.* International Electrotechnical Commission, London.

[27] ISO 6336-3:2019. *Calculation of Load Capacity of Spur and Helical Gears - Part 3: Calculation of Tooth Bending Strength*. International Organization for Standardization, Geneva.

[28] Yu, Z., Zhu, C., Tan, J., Song, C., Wang, Y. Fully-coupled and decoupled analysis comparisons of dynamic characteristics of floating offshore wind turbine drivetrain. *Ocean Eng* 247 110639 (2022) **DOI:10.1016/j.oceaneng.2022.110639**.

[29] ISO 12100:2010. Safety of Machinery-General Principles for Design-Risk Assessment and Risk Reduction. International Organization for Standardization, Geneva.

Acknowledgements *The research work in this paper was supported by the National Natural Science Foundation of China (Grant No. 52405067), Science and Technology Research Program of the Education Department of Hubei Province (Grant No. Q20241205), Hubei Provincial Natural Science Foundation of China (Grant No. 2024AFB316) and the Science and Technology Innovation Key R&D Program of Chongqing (Grant No. CSTB2024TIAD-STX0019).*

Received: 2024-12-03, revised: 2025-06-19, accepted: 2025-07-17
as Original Scientific Paper.

Data availability *The data that underpin the results of this research are available for use by other researchers. Additionally, the corresponding author can provide additional raw data upon reasonable request.*

Author contribution *Yao Li: Writing - review & editing, Writing - original draft, Methodology, Data curation, Project administration; Longsheng Li: Writing - original draft, Methodology; Gaoxiang Ni: Writing - review & editing, Supervision; Xinlong Li: Investigation, Formal analysis, Data curation; Kongde He: Investigation, Formal analysis, Data curation. All authors have contributed significantly to this work and thoroughly reviewed and approved the final version of the manuscript.*

Celovita ocena zmogljivosti zobniških prenosov vetrnih turbin z drsnimi ležaji

Povzetek *Ob upoštevanju strukturnih značilnosti in večizvornih vzbujanj zobniških prenosov vetrnih turbin z drsnimi ležaji ta študija oblikuje večtelesni dinamični model visokozmogljivih zobniških prenosov z drsnimi ležaji. Predlagana je celovita metodologija za ocenjevanje zmogljivosti, ki združuje analitični mrežni proces (ANP) z izboljšano metodo mehke celovite ocene (IFCE). Razvit je bil večrazsežen okvir za celovito ocenjevanje zmogljivosti, ki poudarja praktičnost in stroškovno učinkovitost, ter vključuje ciljno, kriterijsko in indikatorsko raven. Ključni kazalniki ocenjevanja v tem okviru vključujejo podporno silo ležaja glavne gredi, zanesljivost prenosnega sistema, koeficient delitve obremenitve, vibracijske značilnosti in gostoto moči. Z uporabo metodologij ANP in IFCE je bila sistematično ocenjena celovita zmogljivost dveh zobniških prenosov vetrnih turbin z drsnimi ležaji.*

Ključne besede *zobniški prenos vetrne turbine z drsnimi ležaji, celovita ocena zmogljivosti, večrazsežni kazalniki ocenjevanja, analitični mrežni proces (ANP), mehka celovita ocena (FCE)*